Electric and magnetic response of hot QCD matter

T. Steinert[*] and W. Cassing

Institut für Theoretische Physik, Universität Giessen, 35392 Giessen, Germany

We study the electric conductivity as well as the magnetic response of hot QCD matter at various temperatures T and chemical potentials μ_q within the off-shell parton–hadron–string dynamics transport approach for interacting partonic systems in a finite box with periodic boundary conditions. The response of the strongly interacting system in equilibrium to an external electric field defines the electric conductivity σ_0, whereas the response to a moderate external magnetic field defines the induced diamagnetic moment $\mu_L\,(T,\mu_q)$ as well as the spin susceptibility $\chi_S(T,\mu_q)$. We find a sizable temperature dependence of the dimensionless ratio σ_0/T well in line with calculations in a relaxation time approach for $T_c < T < 2.5T_c$ as well as an increase of σ_0 with μ_q^2/T^2. Furthermore, the frequency dependence of the electric conductivity $\sigma(\Omega)$ shows a simple functional form well in line with results from the dynamical quasiparticle model. The spin susceptibility $\chi_S(T,\mu_q)$ is found to increase with temperature T and to rise $\sim\mu_q^2/T^2$ too. The actual values for the magnetic response of the QGP in the temperature range below 250 MeV show that the QGP should respond diamagnetically in actual ultrarelativistic heavy-ion collisions since the maximal magnetic fields created in these collisions are smaller than $B_c(T)$, which defines a boundary between diamagnetism and paramagnetism.

I. INTRODUCTION

The phase diagram of strongly interacting hadronic/partonic matter has been a subject of primary interest in the physics community for decades. At vanishing (or low) chemical potentials, lattice QCD (lQCD) calculations have provided reliable results on the equation of state [1,2] and given a glance at the transport properties, in particular, in the partonic phase. On the other hand, high-energy heavy-ion reactions are studied experimentally and theoretically to obtain information about the properties of nuclear matter under the extreme conditions of high baryon density and/or temperature. Ultrarelativistic heavy-ion collisions at the Relativistic Heavy-Ion Collider (RHIC) and the Large Hadron Collider (LHC) at CERN have produced a new state of matter, strongly interacting quark-gluon plasma, for a couple of fm/c at volumes up to a few 10^3 fm^3 in central reactions. The produced QGP shows features of a strongly interacting fluid unlike a weakly interacting parton gas [3] as had been expected from perturbative QCD. Large values of the observed azimuthal asymmetry of charged particles in momentum space [4–8], i.e., the elliptic flow v_2, could quantitatively be well described by ideal hydrodynamics up to transverse momenta of the order of 1.5 GeV/c [9–14]. Recent studies of "QCD matter" in equilibrium—using lQCD calculations [15,16] or partonic transport models in a finite box with periodic boundary conditions [17,18]—have demonstrated that the ratio of the shear viscosity to the entropy density η/s should have a minimum close to the critical temperature T_c, similar to atomic and molecular systems [19]. On the other hand, the ratio of the bulk viscosity to the entropy density ζ/s should have a maximum close to T_c [18] or might even diverge at T_c [20–24]. Indeed, the minimum of η/s at $T_c \approx 160$ MeV

is close to the lower bound of a perfect fluid with $\eta/s = 1/(4\pi)$ [25] for infinitely coupled supersymmetric Yang-Mills gauge theory (based on the AdS/CFT duality conjecture). This suggests the "hot QCD matter" to be the "most perfect fluid" [26–28]. On the empirical side, relativistic viscous hydrodynamic calculations (using the Israel-Stewart framework) also require a very small η/s, 0.08–0.24, in order to reproduce the RHIC elliptic flow v_2 data [29–32]; these phenomenological findings thus are in accord with the theoretical studies of η/s in Refs. [18,33,34].

Whereas the shear and bulk viscosities of hot QCD matter at finite temperature T presently are roughly known, the electric conductivity σ_0 is a further macroscopic quantity of interest [35,36] since it controls the electromagnetic emissivity of the plasma. First results of lattice calculations on the electromagnetic correlator have provided results that varied by more than an order of magnitude [37–41]. Furthermore, the conductivity dependence on the temperature T (at $T > T_c$) is widely unknown too. The electric conductivity σ_0 is also important for the creation of electromagnetic fields in ultrarelativistic nucleus-nucleus collisions from partonic degrees of freedom, since σ_0 specifies the imaginary part of the electromagnetic (retarded) propagator and leads to an exponential decay of the propagator in time, $\sim\exp(-\sigma_0(t-t')/(\hbar c))$ [42].

Apart from the electric conductivity, the magnetic response of the QGP (or strong vacuum) to external magnetic fields **B** has also been of current interest from the experimental point of view [43–48] as well as from lQCD [49–52]. Strong magnetic fields are created in peripheral relativistic nucleus-nucleus collisions by the charges of the spectator protons during the passage time of the nuclei [48,53,54], and at the top RHIC energy of $\sqrt{s_{NN}} = 200$ GeV magnetic fields of order $eB \approx 5m_\pi^2$ can be reached. This has led to the suggestion of a charge separation effect due to the chiral magnetic effect in these reactions [43–48]. On the other hand, lQCD has been focusing on the magnetic catalysis of the chiral $\langle q\bar{q}\rangle$ condensate at

---

*Thorsten.Steinert@theo.physik.uni-giessen.de

very strong **B** fields and low temperatures and the inverse magnetic catalysis of the chiral condensate at temperatures close to the critical temperature, indicating a decrease in T_c for high magnetic fields. Note, however, that these studies involve time-independent magnetic fields that are significantly higher than those achieved in peripheral nucleus-nucleus collisions for very short times where an equilibrated QGP might not have been established. Nevertheless, a sufficient knowledge of the electric and magnetic response of the QGP (in equilibrium) to external electromagnetic fields is mandatory to explore the possible generation of the chiral magnetic effect in predominantly peripheral heavy-ion reactions [43–48] and to determine the photon production from the QGP in heavy-ion collisions at different centralities and bombarding energies [55–57].

In this work we extend our previous studies on the electric conductivity $\sigma_0(T)$ [58,59] for "infinite parton matter" also to finite quark chemical potential μ_q employing the parton–hadron–string dynamics (PHSD) transport approach [60], which is based on generalized transport equations derived from the off-shell Kadanoff-Baym equations [61,62] for Green's functions in phase-space representation (beyond the quasiparticle approximation). This approach describes the full evolution of a relativistic heavy-ion collision from the initial hard scatterings and string formation through the dynamical deconfinement phase transition to strongly interacting quark-gluon plasma as well as hadronization and the subsequent interactions in the expanding hadronic phase. In the hadronic sector PHSD is equivalent to the hadron–string dynamics transport approach [63–66]—a covariant extension of the Boltzmann-Uehling-Uhlenbeck) approach [67]—that has been used for the description of pA and AA collisions from lower Schwerionen-Synchrotron to RHIC energies in the past. On the other hand, the partonic dynamics in PHSD is based on the dynamical quasiparticle model (DQPM) [68–70], which describes QCD properties in terms of single-particle Green's functions (in the sense of a two-particle irreducible approach) and reproduces lQCD results—- including the partonic equation of state—in thermodynamic equilibrium. For further details on the PHSD off-shell transport approach and hadronization, we refer the reader to Refs. [17,60,71], and [72].

The layout of our study is as follows: In Sec. II we concentrate on calculating the electric conductivity for "infinite" QCD matter also at finite quark chemical potential μ_q and provide simple parametrizations for the dependence of σ_0 on μ_q. Furthermore, we calculate the frequency dependence $\sigma(\Omega)$ for periodic external fields and compare the results with those from the DQPM. In Sec. III we compute the diamagnetic and paramagnetic contributions to the magnetization M of the plasma as a function of the temperature T and μ_q and compare the results to the experimental situation at the RHIC. A summary and discussion of results is presented in Sec. IV.

II. ELECTRIC CONDUCTIVITY

We briefly recall the setup of our studies within PHSD. The "infinite" hadronic or QCD matter is simulated within a cubic box with periodic boundary conditions at various values for the energy density (or temperature) and the quark chemical potential μ_q. The size of the box is fixed to $V = 9^3$ fm^3 as in the

previous investigations [17,18,58]. The initialization is done by populating the box with light (u,d) and strange (s) quarks, antiquarks, and gluons slightly out of equilibrium. The system approaches kinetic and chemical equilibrium during its time evolution within PHSD. For more details on the simulation of equilibrated partonic systems using PHSD in the box at finite temperature T and quark chemical potential μ_q, we refer the reader to Ref. [17].

We recall that PHSD is an off-shell transport approach that propagates quasiparticles with broad spectral functions. Numerically, the continuous spectral distribution in the mass of a particle (given by its spectral function) is probed by a large number of test particles with (evolving) masses $M_j(t)$. In order to include the effects from an external electric field **E** or magnetic field **B**, the propagation of each charged test particle j is performed with the additional Lorentz force in the equation of motion,

$$\frac{d}{dt}\mathbf{p}^j = q_j e \left(\mathbf{E} + \frac{\mathbf{p}^j}{E^j} \times \mathbf{B} \right), \qquad (1)$$

where q_j denotes the fractional charge of the test particle $(\pm 1/3, \pm 2/3)$, and E^j its energy. We recall that the external electric field will lead to an acceleration of positively and negatively charged particles in opposite directions, while the particle scatterings/interactions will damp this acceleration and eventually lead to an equilibrium current (cf. Fig. 1 in Ref. [58]). The electric current density $j_z(t)$ (for an external electric field in the z direction) is calculated by

$$j_z(t) = \frac{1}{VN} \sum_{k=1}^{N} \sum_{j=1}^{N_k(t)} e q_j \frac{p_z^j(t)}{M_j(t)}, \qquad (2)$$

where $M_j(t)$ is the mass of the test particle j at time t. The summation in (2) is carried out over N ensemble members,
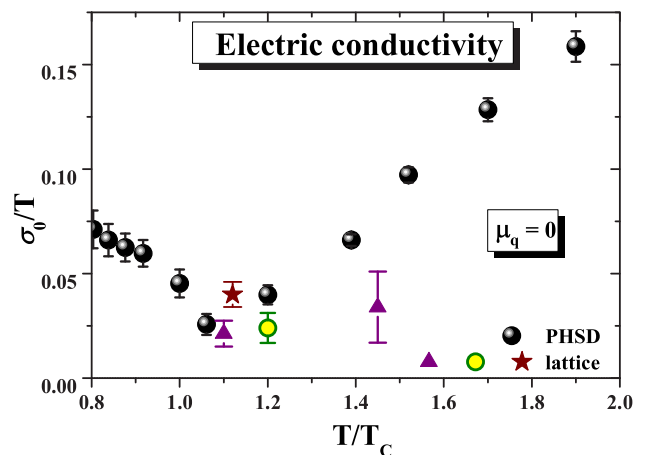

FIG. 1. (Color online) Dimensionless ratio of electric conductivity to temperature σ_0/T, (3), as a function of the scaled temperature T/T_c for $\mu_q = 0$ in comparison with recent lattice QCD results. Triangles, quenched QCD results in the continuum limit with Wilson-Clover fermions and renormalized vector currents [37]; star, quenched SU(2) lattice gauge theory [40]; lightly filled (yellow) circles, QCD with two dynamical flavors of Wilson-Clover fermions [41]. PHSD results (filled black circles) are the same as in Ref. [58].

$k = 1 \ldots N$, while $N_k(t)$ denotes the time-dependent number of "physical" (u,d,s) quarks and antiquarks that varies with time t due to the processes $q + \bar{q} \leftrightarrow g \leftrightarrow q' + \bar{q}'$ in a single member of the ensemble (run). The number of runs N is typically taken as a few hundred, which gives a current $j_z(t)$ practically independent of the number of ensemble members N. We recall that (without external fields) each run of the ensemble is a microcanonical simulation of the dynamics as inherent in the PHSD transport approach, which strictly conserves the total four-momentum as well as all discrete conservation laws (e.g., net fermion number for each flavor) [17]. A note of caution must be given since, due to the external field, we deal with an open system with increasing energy density (temperature) in time. Therefore we employ sufficiently small external fields eE_z such that the energy increase during the computation time (in each run) stays below 2% and the increase in temperature below 1 MeV.

A. Constant electric fields

We find that for constant electric fields up to $eE_z = 50$ MeV/fm a stable electric current j_{eq} emerges that is $\sim E_z$ (cf. Ref. [58]). Accordingly, we obtain the conductivity $\sigma_0(T,\mu_q)$ from the ratio of the stationary current density j_{eq} and the electric field strength as

$$\frac{\sigma_0(T,\mu_q)}{T} = \frac{j_{\text{eq}}(T,\mu_q)}{E_z T}. \qquad (3)$$

The results for the dimensionless ratio, (3), at $\mu_q = 0$ (from Ref. [58]) are displayed in Fig. 1 as a function of the scaled temperature T/T_c in comparison to more recent lQCD results from Refs. [37,40,41] and suggest a minimum at the ratio $\sigma_0(T,\mu_q = 0)/T$ close to the critical temperature T_c, followed by an approximate linear rise up to $2T_c$ (cf. Ref. [58]). The most recent lQCD results [37,40,41] are roughly compatible with the PHSD calculations. Moreover, the lattice data from Ref. [73] give support for the linearity of σ_0/T at a temperature above T_c.

We now focus on the explicit dependence of $\sigma_0(T,\mu_q)/T$ as a function of the chemical potential μ_q, which is shown in Fig. 2 for a fixed temperature $T = 200$ MeV. The numerical result can be fitted with a quadratic correction (solid line in Fig. 2),

$$\frac{\sigma_0(T,\mu_q)}{T} = \frac{\sigma_0(T,\mu_q = 0)}{T}\left(1 + a(T)\mu_q^2\right), \qquad (4)$$

with $a(T) \approx 11.6$ GeV^{-2} for $T = 0.2$ GeV. This result comes about as follows: We recall that the electric conductivity of gases, liquids, and solid states is described in the relaxation time approach by the Drude formula

$$\sigma_0 = \frac{e^2 n_e \tau}{m_e^*}, \qquad (5)$$

where n_e denotes the density of nonlocalized charges, τ is the relaxation time of the charge carriers in the medium, and m_e^* is their effective mass. This expression can be directly computed for partonic degrees of freedom within the DQPM, which was used to match in PHSD the quasiparticle properties to lQCD results in equilibrium for the equation of state as well as various correlators [68–70]. We note that the electromagnetic
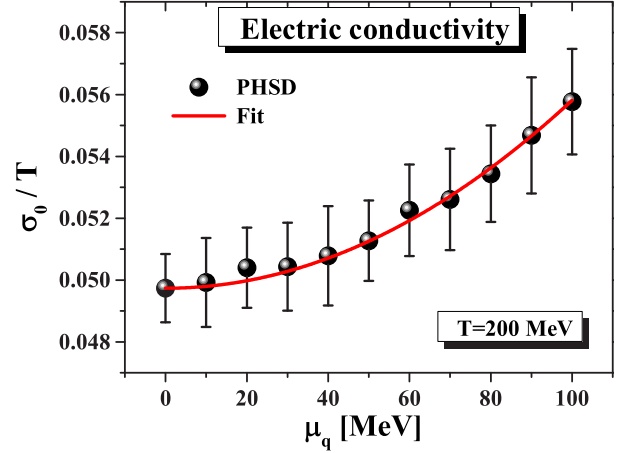

FIG. 2. (Color online) Electric conductivity over temperature σ_0/T as a function of the chemical potential μ_q for $T = 200$ MeV from PHSD calculations (filled black circles). Error bars indicate the statistical uncertainty for the ratio, (3), in calculations for different external field strengths eE_z up to 50 MeV/fm.

correlator from lQCD calculations [37] appears to match rather well the back-to-back dilepton rate from PHSD at $T = 1.45T_c$ (cf. Fig. 2 in Ref. [74]), which suggests that the results of our calculations for σ_0—for vanishing invariant mass—should also be close to the lQCD extrapolations from [37].

In the DQPM, the relaxation time for quarks/antiquarks is given by $\tau = 1/\Gamma_q(T,\mu_q)$, where $\Gamma_q(T,\mu_q)$ is the width of the quasiparticle spectral function (cf. [68] and [71]). Furthermore, the spectral distribution for the mass of the quasiparticle has a finite pole mass $M_q(T,\mu_q)$ that is also fixed in the DQPM, as well as a density of $(u,\bar{u},d,\bar{d},s,\bar{s})$ quarks/antiquarks as a function of temperature and chemical potential (cf. Refs. [68] and [71]). Thus, we obtain for the dimensionless ratio, (3), the expression [58]

$$\frac{\sigma_0(T,\mu_q)}{T} \approx \frac{2}{9}\frac{e^2 n_{q+\bar{q}}(T,\mu_q)}{M_q(T,\mu_q)\Gamma_q(T,\mu_q)T}, \qquad (6)$$

where $n_{q+\bar{q}}(T,\mu_q)$ denotes the total density of quarks and antiquarks and the prefactor $2/9$ reflects the flavor averaged fractional quark charge squared $(\sum_f q_f^2)/3$. As found in our previous study [58] the DQPM results match well with the explicit PHSD calculations in the box for $\mu_q = 0$ since PHSD in equilibrium is a suitable transport realization of the DQPM [17].

In the DQPM we have $\Gamma_q(T,\mu_q) \approx \Gamma_q(T,\mu_q = 0)$ and $M_q(T,\mu_q) \approx M_q(T,\mu_q = 0)$ for $\mu_q \leqslant 100$ MeV, however,

$$n_{q+\bar{q}}(T,\mu_q) \approx n_{q+\bar{q}}(T,\mu_q = 0)\left(1 + a(T)\mu_q^2\right), \qquad (7)$$

with the same coefficient $a(T)$ as in Eq. (4). This is demonstrated explicitly in Fig. 3, where the actual DQPM results for the quark + antiquark density (filled black circles) are compared to the fit, (7) (solid line).

The temperature dependence of the expansion coefficient $a(T)$ is found to be $\sim 1/T^2$ such that the ratio σ_0/T can be
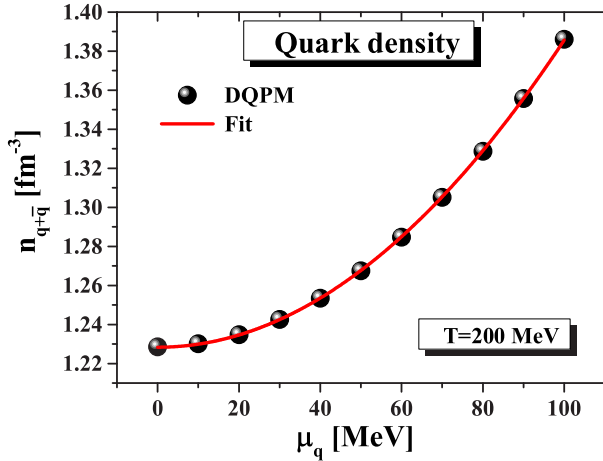
FIG. 3. (Color online) Quark + antiquark density from the DQPM (filled black circles) as a function of the quark chemical potential μ_q for $T = 200$ MeV. The solid (red) line displays the fit, (7), to the DQPM results.

approximated by

$$\frac{\sigma_0(T,\mu_q)}{T} \approx \frac{\sigma_0(T,\mu_q = 0)}{T}\left(1 + c_{\sigma_0}\frac{\mu_q^2}{T^2}\right). \quad (8)$$

In Fig. 4 we display the coefficient c_{σ_0} in the temperature range $170\,\text{MeV} \leqslant T \leqslant 250$ MeV giving $c_{\sigma_0} \approx 0.46$ as the best fit. This completes our study of the stationary electric conductivity σ_0.

B. Periodic electric fields

We now extend our study to external periodic fields of frequency Ω:

$$E_z(t) = E_z^0 \sin(\Omega t). \quad (9)$$

In this case the electric current density $j_z(t)$ does not achieve a constant equilibrium value and also oscillates with the frequency Ω. Figure 5 shows the time dependence of the current $j_z(t)$ from PHSD for different frequencies as a function
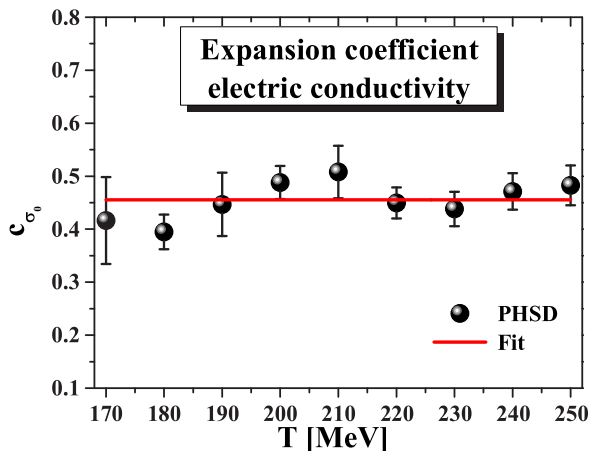

FIG. 4. (Color online) Expansion factor c_{σ_0} in (8) as a function of temperature T for $\mu_q \leqslant 100$ MeV. The solid line shows the average value in the interval $170\,\text{MeV} < T < 250$ MeV.
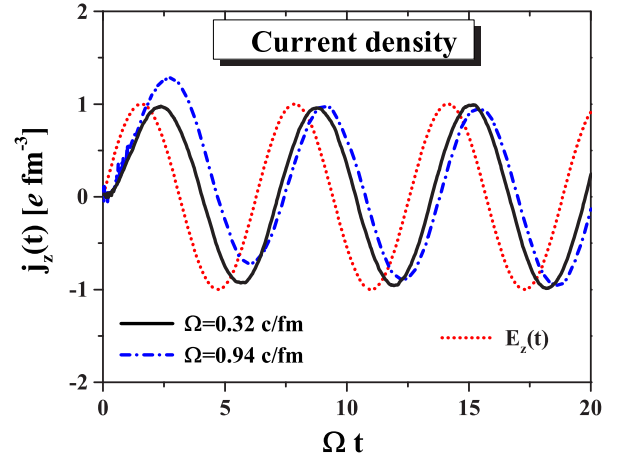

FIG. 5. (Color online) Time-dependent electric current density $j_z(t)$ for $\Omega = 0.32\,c/\text{fm}$ (solid black line) and $\Omega = 0.94\,c/\text{fm}$ [dash-dotted (blue) line] normalized to the equilibrium amplitude for temperature $T = 190$ MeV and $eE_z^0 = 0.005$ GeV$^2 \approx 25$ MeV/fm. The dotted (red) line shows the time dependence of the external electric field $E_z(t)$.

of Ωt, with their amplitudes normalized to 1 in comparison with the external electric field $E_z(t)$ [dotted (red) line]. The current $j_z(t)$ is seen to be shifted in phase compared to the electric field; the phase shift δ increases with the frequency Ω up to $\pi/2$. The currents in Fig. 5 can be well described by

$$j_z(t) = A(\Omega)j_{\text{eq}}\sin(\Omega t - \delta(\Omega)). \quad (10)$$

We find that the amplitude $A(\Omega)$ decreases with the frequency Ω since the current has less time to build up and to follow the external field. This behavior is in line with the complex conductivity $\sigma(\Omega)$ for oscillating fields,

$$\sigma(\Omega) = \frac{\sigma_0}{1 - i\Omega/\Gamma_q} = \frac{\sigma_0}{1 + \Omega^2/\Gamma_q^2} + i\frac{\sigma_0\Omega/\Gamma_q}{1 + \Omega^2/\Gamma_q^2}, \quad (11)$$

where Γ_q is the quasiparticle width of the charged particles (quarks and antiquarks). We have computed the current $j_z(t)$ for $T = 190$ MeV and $eE_z^0 = 0.005$ GeV$^2 \approx 25$ MeV/fm in the frequency range $0.02\,c/\text{fm} < \Omega < 25\,c/\text{fm}$. Figure 6 shows the phase shift $\delta = \arctan(\Omega/\Gamma_q)$, and Fig. 7 the amplitude $A(\Omega) = 1/\sqrt{1 + \Omega^2/\Gamma_q^2}$ (filled black circles). The PHSD results can be easily followed up within the DQPM results [shown by the solid (red) lines], which again provide a good description of the microscopic calculations. Since the complex conductivity $\sigma(\Omega)$ depends only on the width Γ_q and the stationary conductivity σ_0, in (11) its actual values for different temperatures T and finite chemical potential μ_q follow directly from our previous results in this section. Note that for actual electric fields in peripheral Au + Au collisions at the top RHIC energy we have $\Omega \approx 22\,c/\text{fm}$ such that the electric conductivity $\sigma(\Omega)$ is suppressed relative to its equilibrium value by more than a factor of 100.

III. MAGNETIC RESPONSE

In order to explore the magnetic response of the partonic system within PHSD we assume the magnetic field to be
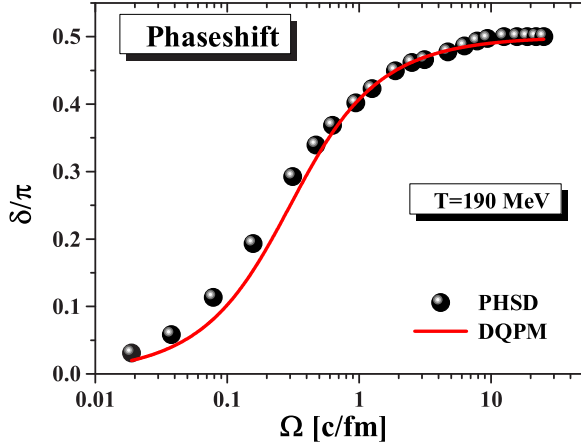
FIG. 6. (Color online) Phase shift δ over π as a function of the frequency Ω from the PHSD calculations (filled black circles) for $T = 190$ MeV. The solid (red) line shows the phase shift as expected from the DQPM using (11).

sufficiently small such that terms $\sim B^2$ can be neglected (see below). Note that this limit does not hold for the strong fields $eB(\sim 0.1$–1 GeV$^2 \approx 0.5$–5 GeV/fm) in actual lQCD studies [50–52]. Using

$$(\boldsymbol{\sigma} \mathbf{D})^2 = \mathbf{D}^2 - qe\boldsymbol{\sigma} \cdot \mathbf{B}, \quad \mathbf{D}^2 = (\mathbf{p} - qe\mathbf{A})^2 = \mathbf{p}^2 - qe\mathbf{L} \cdot \mathbf{B},$$
(12)

with the Pauli matrices $\boldsymbol{\sigma}$, the kinetic momentum $\mathbf{p}$, and the angular momentum $\mathbf{L}$, the Dirac equation can be rewritten for two-component quark and antiquark spinors leading to the Hamiltonian

$$H_{\text{Dirac}} = \sqrt{\mathbf{p}^2 + m^2 - qe(\mathbf{L} + \boldsymbol{\sigma}) \cdot \mathbf{B}}$$
$$\approx E - \frac{qe}{2E}(\mathbf{L} + \boldsymbol{\sigma}) \cdot \mathbf{B} = E - \frac{qe}{2E}(\mathbf{L} + 2\mathbf{S}) \cdot \mathbf{B},$$
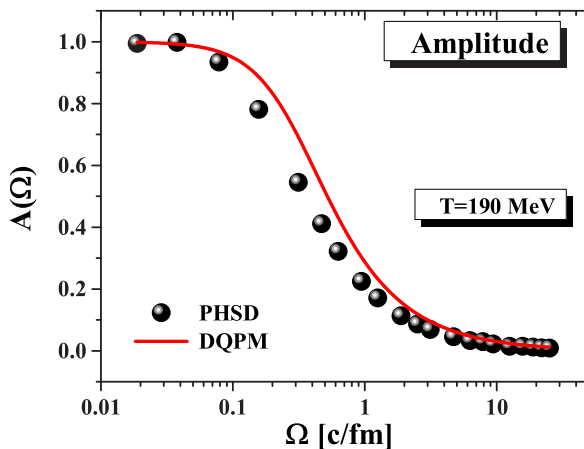(13)

FIG. 7. (Color online) Amplitude $A(\Omega)$ as a function of the frequency Ω from the PHSD calculations (filled black circles) for $T = 190$ MeV. The solid (red) line shows the expected amplitude within the DQPM.

with $E = \sqrt{\mathbf{p}^2 + m^2}$. In the case of low energies $E \to \frac{\mathbf{p}^2}{2m} + m$ this leads to the well-known expression for the nonrelativistic Pauli equation:

$$H_{\text{Pauli}} = \frac{\mathbf{p}^2}{2m} - \frac{qe}{2m}(\mathbf{L} + \boldsymbol{\sigma}) \cdot \mathbf{B}.$$
(14)

The change in the energy of the system in the presence of an external magnetic field $\mathbf{B}$ is determined by the magnetic moment $\boldsymbol{\mu}$,

$$\boldsymbol{\mu} = \boldsymbol{\mu}_L + \boldsymbol{\mu}_S = \frac{qe}{2E}(\mathbf{L} + 2\mathbf{S}),$$
(15)

which has a contribution from the angular momentum $\mathbf{L}$ of a particle and from the spin $\mathbf{S} = \boldsymbol{\sigma}/2$. In the following we investigate both terms separately since they provide contributions to the magnetic moment of opposite sign. In analogy to Sec. II we are dealing with an open system but the increase in the total energy stays below 1%.

A. Diamagnetic contribution

The induced angular momentum $\mathbf{L}$ emerges from the Lorentz force, (1), on a charged particle due to an external field $\mathbf{B}$,

$$\mathbf{F}_L = \frac{qe}{E}(\mathbf{p} \times \mathbf{B}),$$
(16)

and induces a magnetic moment opposite to the direction of the $\mathbf{B}$ field since the charged particle spirals around the magnetic field at frequency $\omega = \frac{qeB}{E} = \frac{p_\perp}{ER}$, where $p_\perp$ is the momentum component of the particle perpendicular to the direction of the magnetic field and R is the radius of the spiral. We obtain alternatively for the angular momentum

$$\mathbf{L} = \frac{Rqe}{|\mathbf{F}_L|E}(\mathbf{p}(\mathbf{p} \cdot \mathbf{B}) - \mathbf{B}\mathbf{p}^2),$$
(17)

where $\mathbf{p}(\mathbf{p} \cdot \mathbf{B})$ is the projection of the momentum in the direction of the magnetic field $\mathbf{e}_B$. Inserting the expression for the radius R we get

$$\mathbf{L} = \frac{-p_\perp^3}{|\mathbf{F}_L|E}\text{sign}(q)\mathbf{e}_B.$$
(18)

Assuming the magnetic field to be oriented in the y direction and employing the Lorentz force $|\mathbf{F}_L| = \frac{|qeB|}{E}p_\perp$, we end up with

$$L_y = \frac{-p_\perp^2}{qeB}.$$
(19)

This gives the induced magnetic moment

$$\mu_L = \frac{-p_\perp^2}{2BE}.$$
(20)

Since the Lorentz force changes only the direction of $\mathbf{p}$, and not its magnitude $|\mathbf{p}|$, the particle energy E is conserved too. As a consequence, the energy contribution in Hamiltonian (13) is independent of the magnetic field strength:

$$\Delta E_{\text{mag},L} = -\mu_L B = -\frac{-p_\perp^2}{2BE}B = \frac{p_\perp^2}{2E}.$$
(21)

We note that the diamagnetic contribution cannot be seen in approaches that calculate the magnetization by differentiation of the thermodynamic potential (e.g., free energy F) with respect to the magnetic field B. In principle, the angular momentum $\mathbf{L}$ has to be quantized. However, the actual values for $\mathbf{L}$ (in units of $\hbar$) are $\gg 1$ for "low" field strengths since $|\mathbf{L}| \sim 1/(eB)$ such that quantum corrections are subleading in our case.

B. Paramagnetic contribution

The quark and antiquark spins provide a paramagnetic contribution since the spin precession around the direction of the magnetic field $\mathbf{B}$ in thermal equilibrium gives a positive magnetic moment μ_S because the energy becomes reduced according to Eq. (13). The spin degrees of freedom is introduced in PHSD in line with the generalized test-particle ansatz [62] for the Wightman function,

$$
iG^{<}(X,P,S) = \frac{1}{N} \sum_{k=1}^{N} \sum_{i=1}^{N_k(t)} \delta^{(3)}(\mathbf{X} - \mathbf{X}_i(t))
$$
$$
\times \delta^{(3)}(\mathbf{P} - \mathbf{P}_i(t))\delta(P_0 - \epsilon_i(t))\delta^{(2)}(\mathbf{S} - \mathbf{S}_i(t)),
$$
(22)

where X and P stand for the space-time and four-momentum coordinates, respectively, while $\mathbf{S}$ denotes the spin degrees of freedom. In (22) the number of ensemble members (runs) is denoted N, whereas N_k is the number of partons in the run $k = 1 \dots N$ that describe the "physical" particles in each microcanonical simulation. The spin degrees of freedom has to be treated in line with quantum mechanics according to the interaction Hamiltonian, (13); i.e.,

$$
\hat{H}_S = -\frac{qe}{2E} \boldsymbol{\sigma} \cdot \mathbf{B}.
$$
(23)

The spin-wave function for a spin-1/2 fermion is taken as a two-component spinor,

$$
|\chi\rangle = \left| \begin{matrix} \uparrow \\ \downarrow \end{matrix} \right\rangle,
$$
(24)

with $\langle \uparrow | \uparrow \rangle$ denoting the probability of spin in the z direction (parallel to the magnetic field), while $\langle \downarrow | \downarrow \rangle$ stands for the probability of an antiparallel orientation. We assume the spin-wave function to be normalized; i.e., $\langle \chi | \chi \rangle = \langle \uparrow | \uparrow \rangle + \langle \downarrow | \downarrow \rangle = 1$. The projection on the coordinate axis i is provided by

$$
S_i = \tfrac{1}{2} \langle \chi | \sigma_i | \chi \rangle.
$$
(25)

The time evolution of the spin projections according to Hamiltonian (23) can be worked out in a straightforward way using

$$
|\chi(t)\rangle = \hat{U}(t,t_0)|\chi(t_0)\rangle = e^{-i\hat{H}_S(t-t_0)}|\chi(t_0)\rangle,
$$
(26)

with

$$
\hat{U}(t,t_0) = \mathbb{1}_2 \cos\left(\frac{qe}{2E}B(t-t_0)\right)
$$
$$
+ i\frac{\boldsymbol{\sigma} \cdot \mathbf{B}}{B} \sin\left(\frac{qe}{2E}B(t-t_0)\right),
$$
(27)

and Eq. (25). The resulting equations of motion lead to a precession of the spin of a quark/antiquark at frequency $\omega = qeB/E$, which changes only if the energy of particle E changes in a collision or in the inelastic reaction $q + \bar{q} \to g \to q' + \bar{q}'$. Since we are using effective interactions, which should be considered an approximation to the resummed interactions, we cannot determine the actual spin of the parton degrees of freedom. For this reason we neglect the spin of the gluons and treat the quark spin statistically. In order to describe an equilibration of the spin degrees of freedom we introduce a spin flip in one-third of the elastic collisions, as motivated by nuclear physics, which favors final spin states parallel to the $\mathbf{B}$ field. In order to simplify the (time-expensive) calculations we introduce the constraint (in equilibrium)

$$
n_\uparrow P_{\uparrow,\downarrow} = n_\downarrow P_{\downarrow,\uparrow} \Longleftrightarrow \frac{P_{\uparrow,\downarrow}}{P_{\downarrow,\uparrow}}
$$
$$
= \frac{n_\downarrow}{n_\uparrow} = \exp(-(E_\downarrow - E_\uparrow)/T) = \exp\left(-\frac{qeB}{ET}\right),
$$
(28)

which is introduced explicitly in the transition matrix element squared. Accordingly, in (28) P denotes the probability of a spin flip and n the occupation probability of a given spin orientation. In practice, the probabilities P are taken as

$$
P_{\downarrow,\uparrow} = 1, \quad P_{\uparrow,\downarrow} = \exp\left(-\frac{qeB}{ET}\right)
$$
(29)

and lead to the proper equilibrium distribution when neglecting the $q + \bar{q} \leftrightarrow g$ channels. Including these channels, we find numerically deviations from the equilibrium distribution by up to 10% since the gluon channels reduce the spin orientation in the direction of the $\mathbf{B}$ field, i.e., induce a "diamagnetic effect." The actual values of the probabilities, (29), are not important for the present study. As long as they fulfill Eq. (28) the equilibrium distribution changes only slightly within statistical error bars. The same holds for the number of collisions with spin flips. Their values are only important for the time scales of the spin equilibration, which, however, we do not address.

The magnetization M is defined by the spin density of the system as

$$
M = \frac{\langle \mu_S \rangle}{V} \approx \chi_S e^2 B,
$$
(30)

which in the case of small magnetic fields eB—as in the present study—is proportional to the strength of the B field, thus defining a magnetic susceptibility χ_S by

$$
\chi_S = \frac{\langle \mu_S \rangle}{e^2 B V}.
$$
(31)

C. Numerical results

In order to explore the range of external magnetic fields eB we can handle reliably within the PHSD calculations for partonic systems, we show in Fig. 8 the energy contribution to the magnetic field, (21), as a function of eB for a temperature $T = 190$ MeV. In fact, the calculations for the energy shift due to the magnetic field eB give constant results for $eB < 50$ MeV/fm—when discarding the spin degrees of
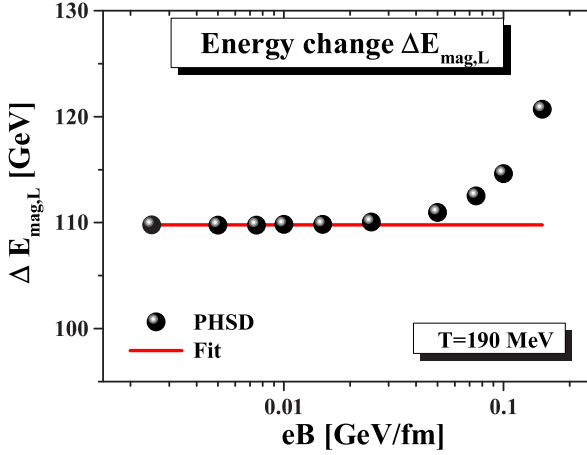
FIG. 8. (Color online) Energy shift due to the magnetic field $\Delta E_{\mathrm{mag},L} = -\mu_L B$ in the PHSD calculation (filled black circles) as a function of the field strength eB for a temperature of $T = 190$ MeV at $\mu_q = 0$. The solid (red) line reflects a constant for small/moderate field strengths.

freedom—while for stronger fields more significant deviations emerge, up to ~10% for eB 200 MeV/fm. Accordingly, we restrict ourselves to $eB \leqslant 50$ MeV/fm (≈ 0.01 GeV^2) in the following.

The temperature dependence of $\Delta E_{\mathrm{mag},L}$ from the PHSD calculation is shown in Fig. 9 by filled black circles and can be well fitted in the interval 170 MeV $\leqslant T \leqslant$ 250 MeV by

$$\Delta E_{\mathrm{mag},L}(T) = 0.3 \cdot (T - 96)^{2.82} \text{ [MeV]}, \tag{32}$$

where the temperature T is given in units of MeV. The diamagnetic contribution to the magnetization from the Lorentz force on the quarks and antiquarks then can be readily extracted by dividing $\Delta E_{\mathrm{mag},L}(T)$ by the strength of the magnetic field.

As the next step we compute the magnetic susceptibility χ_S in the PHSD calculations according to Eq. (31) for different field strengths eB at $\mu_q = 0$. We have found the necessary
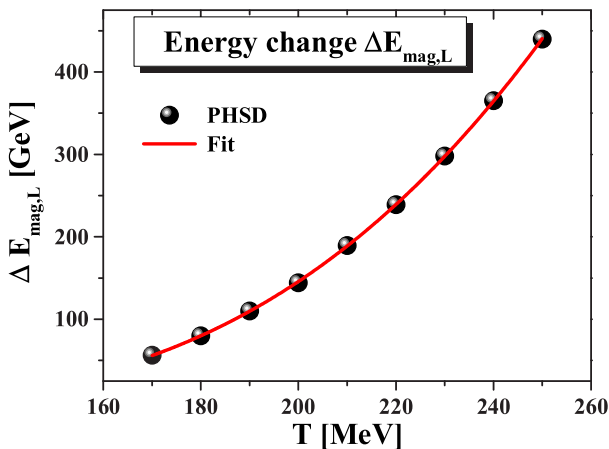

FIG. 9. (Color online) Energy shift due to the magnetic field $\Delta E_{\mathrm{mag},L} = -\mu_L B$ in the PHSD calculation as a function of the temperature T for $\mu_q = 0$. Numerical uncertainties are smaller than the size of the circles. The solid (red) line shows the fit, (32).
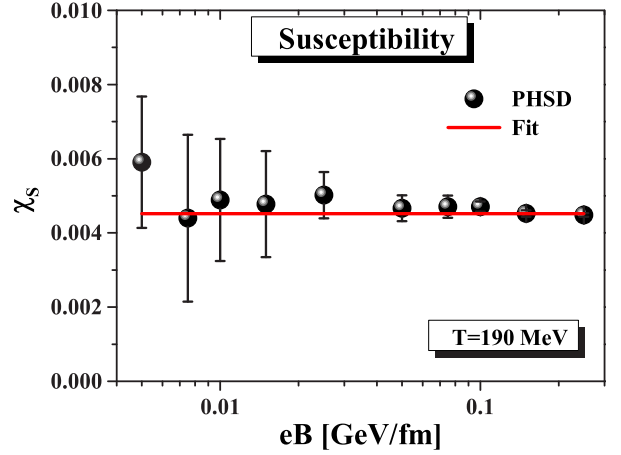

FIG. 10. (Color online) Magnetic susceptibility χ_S, (31), from PHSD as a function of the external magnetic field eB for a temperature $T = 190$ MeV at vanishing quark chemical potential $\mu_q = 0$.

energy for a spin flip to be very low in comparison to the total energy of the quarks ($<1\%$) and therefore have discarded it in our actual simulations. The results for the susceptibility χ_S are displayed in Fig. 10 for $T = 190$ MeV and (within numerical accuracy) show a constant value even up to $eB = 200$ MeV/fm. In this case the numerical accuracy increases with the field strength since the spin-flip probabilities in Eq. (29) differ more significantly for larger magnetic fields. Nevertheless, we have a stable numerical "window" eB from 25 to 50 MeV/fm where the diamagnetic and paramagnetic contributions to the magnetic moment can be calculated with sufficient accuracy. Note that the energy shift due to the paramagnetic contribution is given by

$$\Delta E_{\mathrm{mag},S} = -\chi_S V(eB)^2 \tag{33}$$

and decreases quadratically with the field strength.

The temperature dependence of the magnetic susceptibility $\chi_S(T)$ from PHSD is displayed in Fig. 11 by the filled black circles and can be fitted as

$$\chi_S(T) = 0.017 - \frac{2.39}{T}, \tag{34}$$

with T given in MeV (in the interval 170 MeV $\leqslant T \leqslant$ 250 MeV).

The total energy shift due to both interactions with the magnetic field is given by

$$\Delta E(T,B) = \Delta E_{\mathrm{mag},L}(T) - \chi_S(T)V(eB)^2 \tag{35}$$

and decreases with B^2 at a constant temperature T. At a "critical" field $B_c(T)$ the energy shift changes sign; i.e., for

$$B_c(T) = \sqrt{\frac{\Delta E_{\mathrm{mag},L}}{e^2 \chi_S V}} \tag{36}$$

the magnetization changes from diamagnetic to paramagnetic with increasing magnitude of the field **B**.

This quantity has a minimum (within PHSD) close to the critical temperature $T_c \approx 158$ MeV (cf. Fig. 12) with a minimum $eB_{c,\mathrm{min}} \approx 0.4$ GeV^2 (solid black line; extrapolated
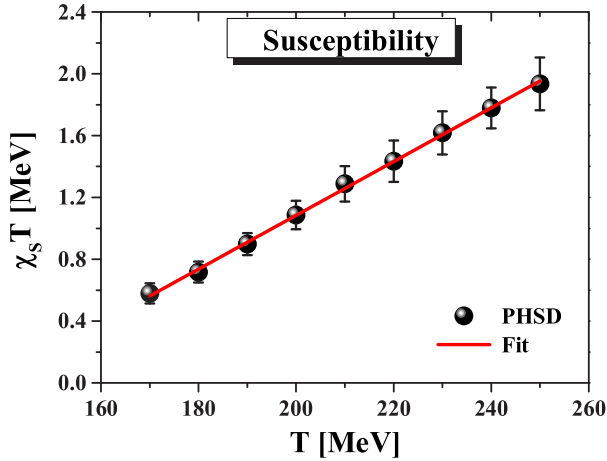
FIG. 11. (Color online) Temperature dependence of the magnetic susceptibility $\chi_S(T)T$ from PHSD (filled black circles) in comparison to the fit, (34), for $\mu_q = 0$. Numerical uncertainties are indicated by the error bars.

FIG. 13. (Color online) Energy shift $\Delta E_{\mathrm{mag},L}(T,\mu_q)$ as a function of μ_q from PHSD (filled black circles) in comparison to the fit, (37), in μ_q [solid (red) line] for $T = 200$ MeV.

by the dashed line according to the fits performed). For comparison we also show the limiting results when assuming all quark/antiquark spins to be oriented in **B** direction. This lower, thin (blue) solid line is slightly lower because the coupling to the gluons (in PHSD) reduces the paramagnetic contribution to the magnetization (diamagnetic gluon effect). In the QGP phase the "critical" field B_c rises with temperature and separates the diamagnetic response (below) from the paramagnetic response (above) of the QGP. Note that the maximal field strength in peripheral Au + Au collisions at the top RHIC energy $\sqrt{s_{NN}} = 200$ GeV was found to be ∼0.09 GeV^2 [53] (solid black horizontal line)—during the

passage time of the nuclei—which is significantly lower than the critical field in Fig. 12. Accordingly, the response of the QGP in actual heavy-ion experiments should be diamagnetic. However, for the much higher field strength explored in lQCD calculations [50–52] for temperatures close to T_c the response should be paramagnetic.

D. Finite quark chemical potential

As in the case of the electric conductivity $\sigma_0(T,\mu_q)$ we can also compute the magnetic response at finite quark chemical potential μ_q in PHSD. In analogy to Fig. 2 we find essentially a quadratic dependence on μ_q as demonstrated in Fig. 13 for $\Delta E_{\mathrm{mag},L}(\mu_q)$ at $T = 200$ MeV. This dependence is also obtained for the magnetic susceptibility $\chi_S(T,\mu_q)$ (not shown explicitly), although with larger numerical error bars.
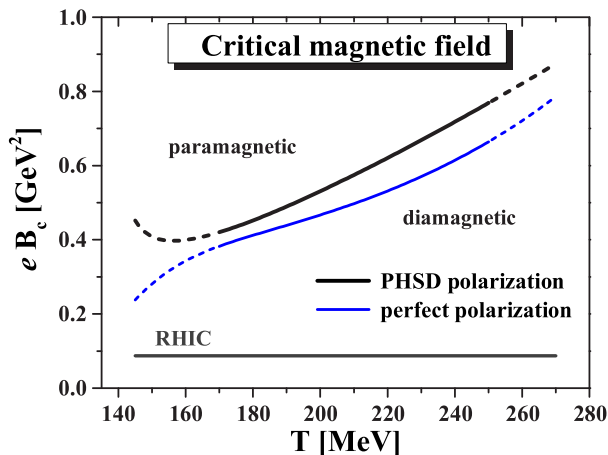

FIG. 12. (Color online) "Critical" magnetic field, (36), as a function of the temperature T for $\mu_q = 0$ from PHSD calculations (solid black line). Dashed extensions are based on the extrapolated fits and not explicitly controlled by PHSD calculations. The lower, thin solid (blue) line results when assuming all quark/antiquark spins to be oriented in the **B** direction. The solid black horizontal line displays the maximum value for the magnetic field strength as found in Ref. [53] at the top RHIC energy.
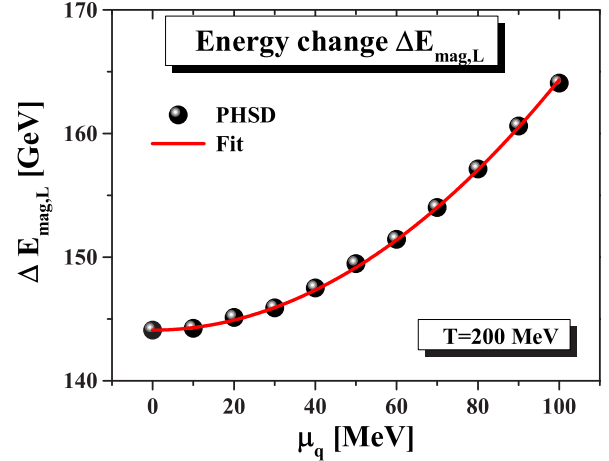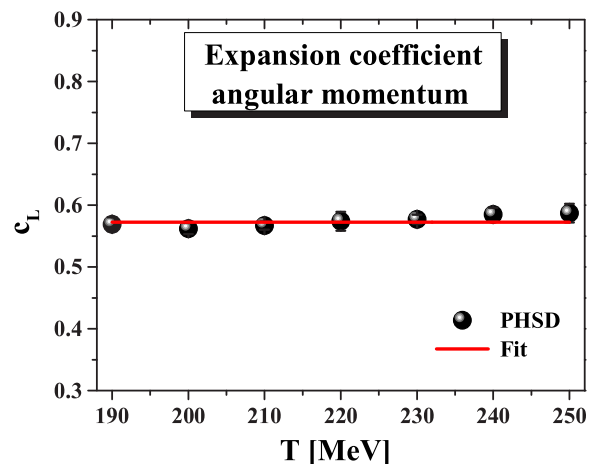

FIG. 14. (Color online) The coefficient c_L in Eq. (37) for $\Delta E_{\mathrm{mag},L}$ in the case of finite $\mu_q \leqslant 100$ MeV as a function of temperature T.

Again, we find the temperature dependence of the coefficient to be $\sim 1/T^2$ such that we get the approximations

$$\Delta E_{\mathrm{mag},L}(T,\mu_q) \approx \Delta E_{\mathrm{mag},L}(T,\mu_q = 0)\left(1 + c_L \frac{\mu_q^2}{T^2}\right),$$

$$\chi_S(T,\mu_q) \approx \chi_S(T,\mu_q = 0)\left(1 + c_S \frac{\mu_q^2}{T^2}\right). \quad (37)$$

As an example we show the coefficient $c_L(T)$ in Fig. 14 for temperatures from 190 to 250 MeV. In this temperature interval the expansion coefficient may be well approximated by $c_L = 0.57$. Similar statements (with less accuracy) hold for the magnetic susceptibility in (37), which gives $c_S = 0.49$. The scaling, (37), can be traced back again to the scaling of the quark + antiquark density $n_{q+\bar{q}}(T,\mu_q)$ in the DQPM.

IV. SUMMARY

In conclusion, we have evaluated the electric conductivity $\sigma_0(T,\mu_q)$ of the QGP as a function of the temperature T and quark chemical potential μ_q by employing the PHSD off-shell transport model in a finite box for the simulation of dynamical partonic systems in equilibrium. The PHSD approach in the partonic sector is based on the lQCD equation of state from [1]; accordingly, it describes the QGP entropy density $s(T)$, the energy density $\varepsilon(T)$, and the pressure $p(T)$ from lQCD [17,60,71] very well. Studies of the QCD matter within PHSD have previously given reasonable results also for the shear and bulk viscosities η and ζ versus T [18] and related transport coefficients [59].

In extension of our previous study in Ref. [58], we have found that the electric conductivity shows a simple scaling with μ_q^2/T^2 [cf. Eq. (8)] which essentially can be traced back to the variation of the quark + antiquark density $n_{q+\bar{q}}$ of the system in the DQPM. We recall that PHSD calculations in a fixed box in equilibrium give practically the same results for the equation of state of QCD matter and transport coefficients as the DQPM [17,18]. In analogy with the ratio of shear viscosity to entropy density η/s we find a clear minimum of the dimensionless ratio σ_0/T in the vicinity of the critical temperature T_c with values close to more recent

lQCD calculations [37,40,41]. This prediction as well as the explicit dependence on μ_q should be controlled by related QCD studies on the lattice. The frequency dependence of the complex electric conductivity $\sigma(\Omega)$ is found to be well in line with the simple results from the DQPM, (11), too.

Furthermore, we have explored the response of the partonic system to a moderate external magnetic field $eB \leqslant 0.1$ GeV/fm and studied separately the diamagnetic response from the Lorentz force, (1), and the paramagnetic response due to the interaction of the quark spin with the magnetic field in Eq. (13). Within the temperature range investigated (170 MeV $< T <$ 250 MeV) the magnetic moment due to the Lorentz force rises with temperature T but drops with $1/B$, providing a constant energy shift due to a coupling to the magnetic field $\Delta E_{\mathrm{mag},L}(\mu_q) > 0$. The coupling of the spin to the B field gives a paramagnetic contribution which can well be characterized by the magnetic susceptibility $\chi_S(T,\mu_q)$. Its contribution to the energy shift of the system is negative and increases with B^2. Accordingly, there is a "critical" magnetic field $B_c(T)$ for which the response of the system changes from diamagnetic to paramagnetic. The actual values for $B_c(T)$ (cf. Fig. 12) demonstrate that the response of the QGP in ultrarelativistic heavy-ion collisions should be diamagnetic since the maximal magnetic fields created in these collisions are smaller than $B_c(T)$. As in the case of the electric conductivity the dependence of the energy shift $\Delta E_{\mathrm{mag},L}(\mu_q)$ as well as the magnetic susceptibility $\chi_S(T,\mu_q)$ shows a very similar scaling correction $\sim \mu_q^2/T^2$ with a coefficient of order 0.5. We close by noting that in the hadronic phase for temperatures below T_c and $\mu_q = 0$ the system dominantly consists of pseudoscalar mesons that have no spin and, accordingly, a low (or vanishing) paramagnetic contribution to the magnetization M when restricted to the first order in the magnetic field. On the other hand, the charged hadrons see the Lorentz force, (1), and build up a diamagnetic contribution.

[1] Y. Aoki, Z. Fodor, S. D. Katz, and K. K. Szabó, Phys. Lett. B **643**, 46 (2006); S. Borsányi, Z. Fodor, C. Hoelbling, S. D. Katz, S. Krieg, C. Ratti, and K. K. Szabó, J. High Energy Phys. 09 (2010) 073; S. Borsányi, G. Endrődi, Z. Fodor, A. Jakovác, S. D. Katz, S. Krieg, C. Ratti, and K. K. Szabó, *ibid.* 11 (2010) 077; S. Borsányi, S. Dürr, Z. Fodor, C. Hoelbling, S. D. Katz, S. Krieg, D. Nógrádi, K. K. Szabó, B. C. Tóth, and N. Trombitás, *ibid.* 08 (2012) 126; S. Borsányi, Z. Fodor, C. Hoelbling, S. D. Katz, S. Krieg, and K. K. Szabó, Phys. Lett. B **730**, 99 (2014).

[2] P. Petreczky (HotQCD Collaboration), PoS LATTICE **2012**, 069 (2012); (HotQCD Collaboration), AIP Conf. Proc. **1520**, 103 (2013).

[3] M. Gyulassy and L. D. McLerran, Nucl. Phys. A **750**, 30 (2005); E. V. Shuryak, *ibid.* **750**, 64 (2005); U. W. Heinz, AIP Conf. Proc.

739, 163 (2004); A. Peshier and W. Cassing, Phys. Rev. Lett. **94**, 172301 (2005).

[4] J. Adams *et al.* (STAR Collaboration), Nucl. Phys. A **757**, 102 (2005).

[5] K. Adcox *et al.* (PHENIX Collaboration), Nucl. Phys. A **757**, 184 (2005).

[6] I. Arsene *et al.* (BRAHMS Collaboration), Nucl. Phys. A **757**, 1 (2005).

[7] B. B. Back *et al.* (PHOBOS Collaboration), Nucl. Phys. A **757**, 28 (2005).

[8] K. Aamodt *et al.* (ALICE Collaboration), Phys. Rev. Lett. **105**, 252302 (2010).

[9] P. Huovinen, P. F. Kolb, U. Heinz, P. V. Ruuskanen, and S. A. Voloshin, Phys. Lett. B **503**, 58 (2001).

[10] P. F. Kolb, P. Huovinen, U. Heinz, and H. Heiselberg, Phys. Lett. B **500**, 232 (2001).

[11] D. Teaney, J. Lauret, and E. V. Shuryak, Phys. Rev. Lett. **86**, 4783 (2001).

[12] T. Hirano and K. Tsuda, Phys. Rev. C **66**, 054905 (2002).

[13] P. F. Kolb and R. Rapp, Phys. Rev. C **67**, 044903 (2003).

[14] P. Huovinen, in *Quark-Gluon Plasma 3*, edited by R. C. Hwa and X.-N. Wang (World Scientific, Singapore, 2004); P. F. Kolb and U. W. Heinz, in *Quark-Gluon Plasma 3*, edited by (World Scientific, Singapore, 2004).

[15] H. B. Meyer, Phys. Rev. D **76**, 101701 (2007).

[16] S. Sakai and A. Nakamura, Pos LAT **2007**, 221 (2007).

[17] V. Ozvenchuk, O. Linnyk, M. I. Gorenstein, E. L. Bratkovskaya, and W. Cassing, Phys. Rev. C **87**, 024901 (2013).

[18] V. Ozvenchuk, O. Linnyk, M. I. Gorenstein, E. L. Bratkovskaya, and W. Cassing, Phys. Rev. C **87**, 064903 (2013).

[19] R. A. Lacey and A. Taranenko, PoS CFRNC **2006**, 021 (2006).

[20] D. Kharzeev and K. Tuchin, J. High Energy Phys. 09 (2008) 093.

[21] F. Karsch, D. Kharzeev, and K. Tuchin, Phys. Lett. B **663**, 217 (2008).

[22] P. Romatschke and D. T. Son, Phys. Rev. D **80**, 065021 (2009).

[23] G. D. Moore and O. Saremi, J. High Energy Phys. 09 (2008) 015.

[24] C. Sasaki and K. Redlich, Phys. Rev. C **79**, 055207 (2009); Nucl. Phys. A **832**, 62 (2010).

[25] G. Policastro, D. T. Son, and A. O. Starinets, Phys. Rev. Lett. **87**, 081601 (2001); P. K. Kovtun, D. T. Son, and A. O. Starinets, *ibid.* **94**, 111601 (2005).

[26] L. P. Csernai, J. I. Kapusta, and L. D. McLerran, Phys. Rev. Lett. **97**, 152303 (2006).

[27] T. Hirano and M. Gyulassy, Nucl. Phys. A **769**, 71 (2006).

[28] B. Jacak and P. Steinberg, Phys. Today **53**, 39 (2010).

[29] P. Romatschke and U. Romatschke, Phys. Rev. Lett. **99**, 172301 (2007).

[30] H. Song and U. W. Heinz, Phys. Rev. C **77**, 064901 (2008).

[31] M. Luzum and P. Romatschke, Phys. Rev. C **78**, 034915 (2008).

[32] B. Schenke, S. Jeon, and C. Gale, Phys. Rev. C **82**, 014903 (2010).

[33] S. Plumari, A. Puglisi, F. Scardina, and V. Greco, Phys. Rev. C **86**, 054902 (2012).

[34] S. Mattiello and W. Cassing, Eur. Phys. J. C **70**, 243 (2010).

[35] Y. Hirono, M. Hongo, and T. Hirano, arXiv:1211.1114.

[36] S. I. Finazzo and J. Noronha, arXiv:1311.6675.

[37] H. T. Ding, A. Francis, O. Kaczmarek, F. Karsch, E. Laermann, and W. Soeldner, Phys. Rev. D **83**, 034504 (2011); O. Kaczmarek *et al.*, PoS Confine. **X**, 185 (2012).

[38] G. Aarts, C. Allton, J. Foley, S. Hands, and S. Kim, Phys. Rev. Lett. **99**, 022002 (2007).

[39] S. Gupta, Phys. Lett. B **597**, 57 (2004).

[40] P. V. Buividovich, M. N. Chernodub, D. E. Kharzeev, T. Kalaydzhyan, E. V. Luschevskaya, and M. I. Polikarpov, Phys. Rev. Lett. **105**, 132001 (2010).

[41] B. B. Brandt, A. Francis, H. B. Meyer, and H. Wittig, PoS Confine. **X**, 112 (2012).

[42] K. Tuchin, Adv. High Energy Phys. **2013**, 490495 (2013).

[43] D. E. Kharzeev, L. D. McLerran, and H. J. Warringa, Nucl. Phys. A **803**, 227 (2008).

[44] D. E. Kharzeev, Ann. Phys. (NY) **325**, 205 (2010).

[45] K. Fukushima, D. E. Kharzeev, and H. J. Warringa, Phys. Rev. D **78**, 074033 (2008).

[46] D. Kharzeev and A. Zhitnitsky, Nucl. Phys. A **797**, 67 (2007).

[47] D. E. Kharzeev and H. J. Warringa, Phys. Rev. D **80**, 034028 (2009).

[48] V. Skokov, A. Illarionov, and V. Toneev, Int. J. Mod. Phys. A **24**, 5925 (2009).

[49] G. S. Bali, F. Bruckmann, G. Endrodi, Z. Fodor, S. D. Katz, S. Krieg, A. Schäfer, and K. K. Szabo, J. High Energy Phys. 02 (2012) 044.

[50] G. S. Bali, F. Bruckmann, M. Constantinou, M. Costa, G. Endrodi, S. D. Katz, H. Panagopoulos, and A. Schäfer, Phys. Rev. D **86**, 094512 (2012).

[51] G. S. Bali, F. Bruckmann, G. Endrodi, F. Gruber, and A. Schäfer, J. High Energy Phys. 04 (2013) 130.

[52] G. S. Bali, F. Bruckmann, G. Endrodi, and A. Schäfer, arXiv:1310.8145.

[53] V. Voronyuk, V. D. Toneev, W. Cassing, E. L. Bratkovskaya, V. P. Konchakovski, and S. A. Voloshin, Phys. Rev. C **83**, 054911 (2011).

[54] V. D. Toneev, V. P. Konchakovski, V. Voronyuk, E. L. Bratkovskaya, and W. Cassing, Phys. Rev. C **86**, 064907 (2012).

[55] H. van Hees, C. Gale, and R. Rapp, Phys. Rev. C **84**, 054906 (2011).

[56] C. Shen, U. Heinz, J.-F. Paquet, and C. Gale, arXiv:1308.2440.

[57] O. Linnyk, V. P. Konchakovski, W. Cassing, and E. L. Bratkovskaya, Phys. Rev. C **88**, 034904 (2013).

[58] W. Cassing, O. Linnyk, T. Steinert, and V. Ozvenchuk, Phys. Rev. Lett. **110**, 182301 (2013).

[59] R. Marty, E. Bratkovskaya, W. Cassing, J. Aichelin, and H. Berrehrah, Phys. Rev. C **88**, 045204 (2013).

[60] W. Cassing and E. L. Bratkovskaya, Nucl. Phys. A **831**, 215 (2009); Phys. Rev. C **78**, 034919 (2008).

[61] L. P. Kadanoff and G. Baym, *Quantum Statistical Mechanics* (Benjamin, New York, 1962).

[62] S. Juchem, W. Cassing, and C. Greiner, Phys. Rev. D **69**, 025006 (2004); Nucl. Phys. A **743**, 92 (2004).

[63] W. Cassing and E. L. Bratkovskaya, Phys. Rep. **308**, 65 (1999).

[64] E. L. Bratkovskaya and W. Cassing, Nucl. Phys. A **619**, 413 (1997).

[65] W. Cassing, Nucl. Phys. A **700**, 618 (2002).

[66] E. L. Bratkovskaya, S. Soff, H. Stöcker, M. van Leeuwen, and W. Cassing, Phys. Rev. Lett. **92**, 032302 (2004).

[67] W. Cassing, V. Metag, U. Mosel, and K. Niita, Phys. Rep. **188**, 363 (1990).

[68] W. Cassing, Nucl. Phys. A **795**, 70 (2007).

[69] W. Cassing, Nucl. Phys. A **791**, 365 (2007).

[70] A. Peshier, Phys. Rev. D **70**, 034016 (2004); J. Phys. G **31**, S371 (2005).

[71] E. L. Bratkovskaya, W. Cassing, V. P. Konchakovski, and O. Linnyk, Nucl. Phys. A **856**, 162 (2011).

[72] W. Cassing, Eur. Phys. J. Spec. Topics **168**, 3 (2009).

[73] A. Amato, G. Aarts, C. Allton, P. Giudice, S. Hands, and J.-I. Skullerud, Phys. Rev. Lett. **111**, 172001 (2013).

[74] O. Linnyk, W. Cassing, J. Manninen, E. L. Bratkovskaya, P. B. Gossiaux, J. Aichelin, T. Song, and C. M. Ko, Phys. Rev. C **87**, 014905 (2013).